

Strongly correlated electron physics in nanotube-encapsulated metallocene chains

V. M. García-Suárez¹, J. Ferrer², and C. J. Lambert¹

¹ *Department of Physics, Lancaster University, Lancaster, LA1 4YB, U. K. and*

² *Departamento de Física, Universidad de Oviedo, 33007 Oviedo, Spain*

(Dated: April 26, 2021)

The structural, electronic and transport properties of metallocene molecules (MCp₂) and isolated or nanotube-encapsulated metallocene chains are studied by using a combination of density functional theory and non-equilibrium Green's functions. The analysis first discusses the whole series of isolated MCp₂ molecules, where $M = V, Cr, Mn, Fe, Co, Ni, Ru, \text{ and } Os$. The series presents a rich range of electronic and magnetic behaviors due to the interplay between the crystal field interaction and Hund's rules, as the occupation of the d shell increases. The article then shows how many of these interesting properties can also be seen when MCp₂ molecules are linked together to form periodic chains. Interestingly, a large portion of these chains display metallic, and eventually magnetic, behavior. These properties may render these systems as useful tools for spintronics applications but this is hindered by the lack of mechanical stability of the chains. It is finally argued that encapsulation of the chains inside carbon nanotubes, that is exothermic for radii larger than 4.5 Å, provides the missing mechanical stability and electrical isolation. The structural stability, charge transfer, magnetic and electronic behavior of the ensuing chains, as well as the modification of the electrostatic potential in the nanotube wall produced by the metallocenes are thoroughly discussed. We argue that the full devices can be characterized by two doped, strongly correlated Hubbard models whose mutual hybridization is almost negligible. The charge transferred from the chains produces a strong modification of the electrostatic potential in the nanotube walls, which is amplified in case of semiconducting and endothermic nanotubes. The transport properties of isolated metallocenes between semi-infinite nanotubes are also analyzed and shown to lead to important changes in the transmission coefficients of clean nanotubes for high energies.

PACS numbers: 85.35.Kt, 85.65.+h, 71.15.Mb, 71.10.Pm

I. INTRODUCTION

Carbon nanotubes¹ have been for long proposed as possible elements for electronic circuits on the nanoscale. Apart from their mechanical stability and small diameter, these devices can be produced in large quantities and be easily assembled. Furthermore, they can be shaped in very different geometric configurations which make them specially suitable to join different parts of a nanocircuit and achieve novel switching features². On the other hand the electronic properties can range from insulating to metallic³ depending on the radius and the chirality. In the absence of defects, electron transport falls in the ballistic regime and therefore large carrier mobility, high yield and low power consumption is expected. Additional functionality can be achieved by promoting defects in the nanotube walls⁶, or by doping them. n - and p -doped nanotubes can be fabricated by pulling charge in or out of the walls^{7,8,9,10,11,12,13,14,15,16}. These functionalities enable the nanotubes to mimic different parts of a transistor^{4,5,6} and even to produce devices with negative differential resistance⁸.

Several methods have been used to produce n - and p -doped SWNTs but most of them have the problem that the resulting SWNTs are not stable upon air exposition due to oxidation processes which tend to p -dope the carbon wall. A better procedure consists of encapsulating¹⁷ metallic atoms¹⁸, or even organic molecules like fullerenes¹⁹ inside the nanotube walls. Metallic elements and compounds tend to form continuous conducting nanowires¹⁷, while fullerenes produce local distortions in the electronic band structure of the nanotube¹⁹. This way, fullerenes can be used to section the nanotube into different segments²⁰. This local change of the gap should effectively produce a series of quantum dots that could local-

ize electrons²¹. Trapping single electrons may be used to produce entangled electron pairs and also to tailor interactions between static and flying qubits²². The type of charge transfer can be traced back to electron affinity and the ionization potential of the encapsulated molecules. It is recognized now that molecules with high electron affinity tend to remove charge from the nanotube wall and produce p -doped SWNTs, whereas molecules with low ionization potential tend to transfer charge to the wall and produce n -doped SWNTs^{23,24}.

Nanotubes can also be rendered magnetically active upon encapsulation of magnetic elements or organometallic molecules. These new devices offer the possibility to separate the magnetic material from the environment and hence reduce its oxidation. Additionally, encapsulation may give rise to new magnetic properties not present in conventional magnetic nanowires²⁵ and even change the mechanical stability of the nanotubes²⁶. These include, for example, hysteresis loop shifts due to exchange bias^{27,28}, changes in the complex permittivity and permeability²⁹, increased coercitivity and Barkhausen jumps³⁰, magnetic anisotropy³¹, size and number-dependent interactions between catalyst particles³² and many other magnetic phenomena. Other fascinating properties include the disappearance of magnetism in small clusters of Ni atoms³⁴ or the antiferromagnetic behavior shown by iron^{35,36}.

The subject-matter of this article is a theoretical proposal for the encapsulation of specific metallorganic molecules in nanotubes, that combine the two functionalities sketched in the former two paragraphs, e. g.: tailored doping and addition of magnetic behavior to carbon nanotubes. The proposed metallorganic molecules are called metallocenes^{38,39} and are composed of a metallic transition metal (TM) atom and two

cyclopentadienyl (Cp) rings made out of five carbon and five hydrogen atoms each. The configuration of both rings is specially stable if they loose an electron, thus transforming in aromatic rings where the π -electrons are delocalized around the ring. This produces a negative compound that can bind to another Cp ring through a TM atom with a valence of +2 or higher. The case with a valence of +4, which is specially relevant for the fabrication of polymers is not dealt with in the present paper. The article instead focuses only on the simplest metallocene molecule structures, which have only two Cp rings bridged by the TM atom. We note that some of these molecules have already been suggested as the functional core of ingenious electronics devices. For instance, FeCp_2 (ferrocene) has recently been proposed as a molecular bridge that can rival the conductance of conjugated molecules^{40,41} and as a molecular switch⁴³. A spintronics switch made out of two CoCp_2 molecules (cobaltocenes), sandwiched by two magnetic leads, has also been proposed⁴². Explicit encapsulation of cobaltocene in carbon nanotubes was recently realized by Li and coworkers³⁷, who showed that such composite devices are stable for nanotube diameters of 9.4 Å. For thicker nanotubes only a modified version of the cobaltocene (bis(ethylcyclopentadienyl)) was observed to remain inside the tube. This was possibly due to the fact that cobaltocenes, which are smaller than bis(ethylcyclopentadienyl), bonded too weakly to the wall of the thicker tubes and were expelled from them at the slightest thermal or mechanical fluctuations. Li and coworkers also reported a charge transfer from the molecule to the nanotube wall and a red shift in the photoluminescence spectra due to the formation of localized impurity states, which could make these systems specially suitable to produce n -doped nanotubes and modulate the electronic properties of the nanotube wall.

Noting that TMCP_2 molecules could be synthesized with $\text{TM}=\text{V, Cr, Mn, Co and Ni}$, as well as Ru and Os , and that each of them display different electronic and magnetic properties, we proposed⁴⁴ to use them as off-the-shell elements to fabricate one-dimensional chains of metallocene molecules, encapsulated inside the carbon nanotubes walls. In other words, we proposed to fabricate nanoscale wires whose tailored electronic, magnetic and conducting properties would be due to the transition metal atoms of the metallocene molecules, and where the major role of the nanotube would be to actually provide mechanical and electric isolation to the metallocene core. We envisioned two possible categories of devices. In the first class, the nanotube walls would also be metallic, and therefore the properties of the device would come from a non-conventional interplay between two non-trivial electron systems. In the second category, the nanotube walls remain semi-conducting, and the analog of a electrical appliance wire on the nanoscale would be realized.

In this article we take further our previous calculations and show a host of additional features that can be present in these systems. We analyze the structural and magnetic properties of isolated metallocene molecules and isolated or encapsulated chains. We confirm that the devices display a rich variety of electronic properties that can indeed be traced back to the diverse filling of the metallocene molecular levels. We find

that the metallocene chains are very accurate realizations of the one-dimensional Hubbard model, with hopping, Hubbard U and doping parameters that can be extracted unequivocally from the simulations. These chains transfer charge to the nanotube walls, but do not hybridize with them. For the metallic nanotube class we therefore find two Hubbard liquids that act as reservoirs of each other. On the contrary, for the semi-conducting nanotube class, and whenever the encapsulation is endothermic (e.g.: when the diameter of the nanotube is small), we find that the metallocene molecules produce significant energy barriers on the nanotube walls that could localize electrons. We believe that these devices may be useful for quantum computation, due to the possibility to realize and tailor interactions of localized and flying qubits²².

The outline of the article is as follows: we describe in Section II our assembly of theoretical methods. The properties of isolated metallocene molecules and chains of metallocenes are shown in Section III. In Sections IV and V we focus on the properties of chains of metallocenes inside nanotubes and the mapping to strongly correlated models. In Section VI we study the transport properties of isolated metallocenes inside carbon nanotubes. We close the article with a section that presents and discusses our conclusions.

II. THEORETICAL METHOD

The calculations were based on Density Functional Theory⁴⁵ as implemented in the first-principles code SIESTA⁴⁶, which uses norm-conserving pseudopotentials⁴⁷ to get rid of the core electrons and linear combinations of localized atomic orbitals $\phi_\mu(\vec{r} - \vec{d}_\mu)$ to span the valence states⁴⁸. The pseudopotentials, which were optimized so that the local part was smooth⁴⁶, also included non-linear core corrections⁴⁹ for the transition metal atoms of the MCP_2 molecules, with core correction radii of 0.70 a. u. These were obtained by following the recipe used to generate the pseudopotential in iron explained in Ref. 50. The basis set had a double- ζ character for carbon and hydrogen atoms and double- ζ polarized for the transition metal atoms. The cutoff radii were determined by minimizing the energy for a given reference system, i. e.: the H_2 molecule for hydrogen, a diamond crystal for carbon, and the bulk phase for the corresponding transition metal atom.

Due to the localized character of the atomic orbitals special care had to be taken to minimize the impact on our results of both the basis set superposition error (BSSE)⁵² and the basis set incompleteness error (BSIE)^{53,54}. The first error comes from the fact that the Hilbert space of the composite system is different from the Hilbert space of the each part taken separately and therefore the binding energy is smaller due to an additional contribution which comes from the the presence of more localized states. In order to correct BSSE, it is necessary then to subtract the additional contribution by calculating in separate simulations the energy of each individual system in the geometry of the composite system, but inserting ghost states at the location of the missing atoms. Then, the binding energy of the device is estimated as

$$\Delta E = \Delta E_0 - (E_{A+GB} - E_A) - (E_{B+GA} - E_B) \quad (1)$$

where A and B represent the nanotube and the molecule in the relaxed configuration of the composite system, GA and GB are the corresponding ghost states and $\Delta E_0 = E_{AB} - E_{A_{\text{rel}}} - E_{B_{\text{rel}}}$ is the binding energy calculated without ghost states and relaxing all structures.

The contribution from the BSIE appears when there is large interstitial separation between different parts of a system which is described with localized basis sets. Although it is not possible to estimate this contribution it is known to have an opposite sign to the BSSE. This implies that the calculated values of the BSSE-corrected binding energy are upper bounds. We note anyway that we were careful enough to span all the interstitial space between the molecule and the nanotube wall so that the states of the molecule and the nanotube wall had enough overlap.

The exchange and correlation energy and potential were calculated with the generalized gradient approximation (GGA) as parameterized by Perdew, Burke and Ernzerhof⁵⁵, since this approximation works much better for transition metal elements^{50,51}. The real space grid used to compute the integrals leading to density and Hamiltonian matrix elements was calculated by setting a plane wave cutoff of 200 Ry. Finally, we took a number of k -points along the direction of the nanotube (z -axis), ranging from 20 to 100, depending on the size of the system and on whether the nanotube was semiconducting or metallic.

The transport properties were obtained with the ab-initio code SMEAGOL⁵⁷, which uses the Hamiltonian provided by SIESTA to calculate the retarded Green's function of the scattering region (M), which in the basis of atomic orbitals is expressed as

$$G_{\text{MM},\mu\nu}^{\text{R}}(E) = [E^+ S - H - \Sigma_{\text{L}}^{\text{R}}(E) - \Sigma_{\text{R}}^{\text{R}}(E)]_{\text{MM},\mu\nu}^{-1} \quad (2)$$

where S is the overlap matrix, H is the Hamiltonian, $E^+ = E + i\delta$ and

$$\Sigma_{\text{L}}^{\text{R}}(E) = [E^+ S - H]_{\text{ML}} G_{\text{LL}}^{\text{R}}(E) [E^+ S - H]_{\text{LM}} \quad (3)$$

$$\Sigma_{\text{R}}^{\text{R}}(E) = [E^+ S - H]_{\text{MR}} G_{\text{RR}}^{\text{R}}(E) [E^+ S - H]_{\text{RM}} \quad (4)$$

are the self-energies that take into account the coupling to the left and right semi-infinite electrodes. $G_{\text{LL(RR)}}^{\text{R}}$ are the surface Green's functions. From the retarded Green's function and its Hermitian conjugate, the advanced Green's function G^{A} , it is possible to obtain the density matrix using the Keldysh formalism⁵⁸, so that

$$\rho_{\mu\nu} = \frac{1}{2\pi i} \int_C dE G_{\text{MM},\mu\nu}^<(E) \quad (5)$$

where $G^<$ is the retarded Green's function, which in general is calculated as

$$G_{\text{MM}}^<(E) = G(E)_{\text{MM}}^{\text{R}} [\Gamma_{\text{L}} f_{\text{L}} + \Gamma_{\text{R}} f_{\text{R}}](E) G(E)_{\text{MM}}^{\text{A}} \quad (6)$$

where $\Gamma_{\text{L(R)}} = i[\Sigma_{\text{L(R)}}^{\text{R}} - \Sigma_{\text{L(R)}}^{\text{A}}]$ are the gamma matrices that take into account the strength of the coupling to the leads and $f_{\text{L(R)}}(E) = f(E - \mu_{\text{L(R)}})$ are the Fermi distribution functions of the leads. Such a procedure is necessary to obtain the electronic density, $n(\vec{r}) = \sum_{\mu,\nu} \rho_{\mu\nu} \phi_{\mu}(\vec{r} - \vec{d}_{\mu}) \phi_{\nu}(\vec{r} - \vec{d}_{\nu})$, because the calculation deals with semi-infinite leads and also in a general non-equilibrium situation the distribution function of the scattering region is not well defined and therefore the common diagonalization procedure can not be used.

Once the self-consistency is achieved the conductances for spin-up and spin-down electrons are calculated by using the familiar expression⁶⁰

$$\mathcal{G}_{\sigma}(E) = \frac{e^2}{h} \text{tr}[\Gamma_{\text{L}} G_{\text{MM}}^{\text{A}} \Gamma_{\text{R}} G_{\text{MM}}^{\text{R}} \Gamma_{\text{R}}]_{\sigma}(E) \quad (7)$$

where $\sigma = \{\uparrow, \downarrow\}$ is the spin index. The current is simply the integral of the conductance multiplied by the difference of the Fermi distribution functions of the leads.

III. ISOLATED TMCP₂ MOLECULES AND CHAINS

As stated above, metallocenes where the transition metal belong to the $3d$ row or the iron column (ruthenocene and osmocene) are composed of a metallic atom sandwiched by two Cp rings. Such rings can be located just one on top of the other, so that the axis that passes through the middle of the rings and the metallic atom is C_5 and therefore the symmetry is an eclipsed D_{5h} , or rotated 36 degrees relative to each other, so that the symmetry is D_{5d} , i. e. staggered, and each carbon or hydrogen atom sits on top of one of the edges of the other ring. In many cases the same metallocene can have both structures depending on the phase. For instance, vanadocene has D_{5d} symmetry in the solid state, but D_{5h} in the gas phase. However, we always found in our calculations the first configuration to be more stable than the second one by an amount that could be as large as 0.03 eV (for the cobaltocene). This difference can be due to the BSIE, that artificially decreases the interaction between the rings. We have anyhow tested for several of the calculations that both geometric arrangements of the Cp rings produce almost identical results. We are therefore confident that this difference is not important for our study.

The theoretical average distance between carbon atoms in the Cp₂ rings is 1.46 ± 0.05 Å, although it can change slightly depending on the type of metallocene. These results compare rather well with experiments, which give an average distance of 1.44 Å for the ferrocene³⁹, for example. The distance between carbon and hydrogen atoms is equal to 1.10 Å. The main structural parameter, which is the distance between TM and carbon atoms is listed in table I, along with the distance between the TM atom and the plane of the Cp ring. In almost all cases the first type of distance is the same for each of

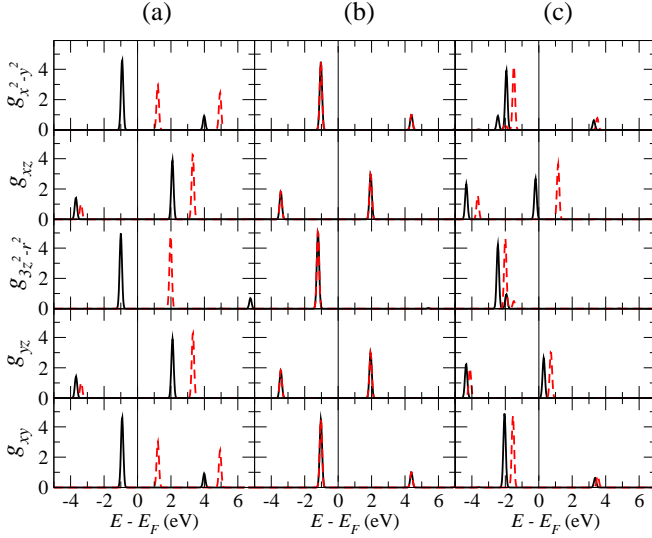


FIG. 1: Densities of States g_i of (a) VCp₂, (b) FeCp₂ and (c) CoCp₂, projected onto the d -shell orbitals of the $3d$ -row metal atom, $i = d_{x^2-y^2}, d_{xz}, d_{3z^2-r^2}, d_{yz}, d_{xy}$. Continuous and dashed lines represent spin-up and spin-down electrons, respectively.

the ten carbon atoms in each metallocene. However, the axis of the two Cp rings in chromocene and, to a lesser extent, in cobaltocene, were found to be tilted, in agreement with experiments, possibly due to the lifting of degeneracy by a Jahn-Teller distortion⁵⁹. The distances in these cases vary between 2.09 and 2.26 Å for CrCp₂, and between 2.07 and 2.15 Å for CoCp₂. Table I shows in these two case the average value. As can be seen the agreement between theory and experiment is excellent, with the only exception of manganocene. The reason of such discrepancy could be due to the fact that the distances for MnCp₂ correspond to the high spin state while we only considered the low spin configuration.

The differences in the electronic structure of the metallocenes can be traced back to the progressive filling of the d -shell of the TM atom, that we also show in table I. These electronic structures are determined by the interplay among electron filling, Hund's rules and the crystal field interaction. To illustrate this, we show in Fig. (1) the density of states projected onto the five d -orbitals of the TM atom, of VCp₂, FeCp₂ and CoCp₂. We find, first, that the d_{xz} and d_{yz} orbitals feel a different crystal field than the rest of orbitals, since they are oriented towards the carbon atoms in the Cp rings. They also overlap strongly with the carbon orbitals and, consequently, their energy levels are split into bonding and antibonding states. These two orbitals are degenerate in energy for all metallocenes, see Fig. (1 (a), (b)). Chromocene and cobaltocene are an exception since, due to the Jahn-Teller distortion the axis of the molecule is bent. Consequently, the degeneracy of the d_{xz} and d_{yz} orbitals is lifted, as shown in Fig. (1 (c)). The energy levels of the $d_{x^2-y^2}$, d_{xy} and $d_{3z^2-r^2}$ are almost degenerate and lie lower in energy because they are not oriented towards the carbon atoms. Additionally, $d_{x^2-y^2}$ and d_{xy} orbitals overlap a little with carbon orbitals, while the $d_{3z^2-r^2}$ does not. Iron d -orbitals in FeCp₂ thereby arrange in

TABLE I: Theoretical and experimental distances between the TM and the carbon atoms, between the carbon atoms and the Cp₂ rings, and number of unpaired electrons. Experimental values from Ref. 39.

Metallocene	Distance TM-C (Å)		Distance TM-Cp (Å)		Unpaired e^-
	This study	Exp.	This study	Exp.	
VCp ₂	2.27	2.28	1.91	1.92	3
CrCp ₂	2.15 (Av.)	2.17	1.79 (Av.)	1.67	2
MnCp ₂	2.07	2.38	1.66	2.14	1
FeCp ₂	2.04	2.06	1.63	1.66	0
CoCp ₂	2.11 (Av.)	2.12	1.71 (Av.)		1
NiCp ₂	2.20	2.20	1.82		2
RuCp ₂	2.21		1.83		0
OsCp ₂	2.21		1.83	1.86	0

a closed shell structure; consequently FeCp₂ has no unpaired electrons and is non-magnetic. The remaining metallocenes display a sort of mirror symmetry about the closed-shell ferrocene. Notice that the exchange splittings, shown in Fig. (1), are proportional to the number of unpaired electrons. It is also interesting to note that the geometric arrangement is such that the orbital angular momentum is quenched, and therefore the measured values of the magnetization almost coincide with the spin moments.

The distribution of electrons in the d orbitals can also explain why the distance between the Cp ring and TM atoms has a minimum for ferrocene. We note that the same behavior is found for the lattice constant of periodic isolated metallocene chains⁴⁴, where the C_5 axis of the molecule and of the chain lie parallel to each other. The electronic band structure of isolated VCp₂ and CoCp₂ chains is plotted in Fig. (2). Notice that VCp₂ chains are semiconducting with a large band gap. Moreover, their bands are essentially flat. This is expected, since metallocene molecules are fairly stable and should show small overlaps among each other. The band structure of CoCp₂ chains is more interesting. First, the band width is larger -of about a quarter of an electron volt- and, second CoCp₂ chains are semiconducting, as expected, but the gap is fairly small. Both chains are strong ferromagnets, since their exchange splittings are such that up- and down-spin bands do not overlap in energy. CoCp₂ chains are therefore more promising for fabrication of transport devices, and this paper shall mostly focus on them henceforth.

We remind that CoCp₂ molecules possess a bent axis, that leads to a lifting of degeneracy of the molecular levels associated to the d_{xz} and d_{yz} orbitals. Fig. (2 (b)) shows that the molecular crystal field also lifts the degeneracy of the one-dimensional bands closest to the Fermi energy, that are associated with these two orbitals. We note that the splitting is of about 0.5 eV. The figure also shows that these two bands are exchange-split by an amount of 1.3 eV for the d_{xz} and 0.4 eV for the d_{yz} . We take now the spin-up and down d_{xz} bands and realize that they may be interpreted as the mean-field ferromagnetic solution of a one-dimensional nearest-neighbors Hubbard model at half-filling, with a hopping integral of 0.06 eV (bandwidth of 0.25 eV), provided that there are no inter-band excitations (e.g.: electrons from the filled majority-spin,

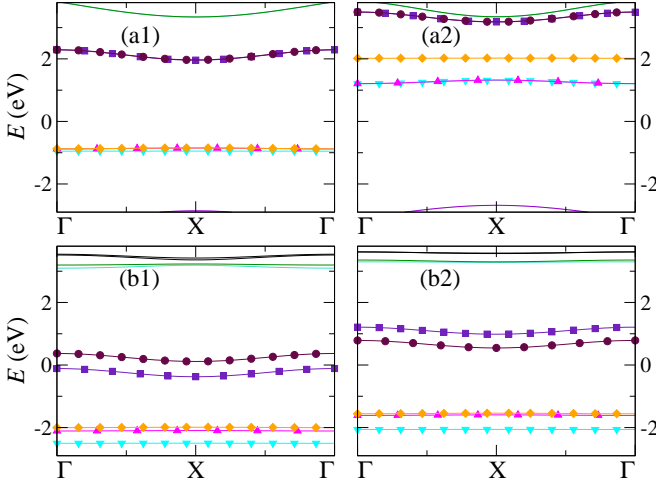


FIG. 2: Band structure around the Fermi level for chains of vanadocene ((a1) and (a2) for majority and minority spin, respectively) and cobaltocene ((b1) and (b2)) calculated at a lattice constant of 7.5 Å. Circles, squares, diamonds, triangles up and triangles down represent d_{yz} , d_{xz} (e_{1g}^* orbitals), $d_{x^2-y^2}$, d_{xy} (e_{2g} orbitals) and $d_{3z^2-r^2}$ (a_{1g}^* orbital), respectively.

d_{xz} band can not be excited to neither of the unfilled majority or minority spin, d_{yz} bands). The coulomb integral U can then be extracted by noting that the spin-splitting is equal to Un , where $n = 1$ is the filling fraction. Hence U is equal to 1.3 eV. But the ground state of a half-filled Hubbard model is not a ferromagnetic metal, but an insulating antiferromagnet. We have therefore simulated helical arrangements of spins^{50,51}. We show in Fig. (3 (a)) the energy of these spin spirals as a function of the wave-vector q of the helix. The figure shows that the ground state is indeed an antiferromagnet. This fact further confirms our belief that these chains are perfect playgrounds of Hubbard physics. A final word of caution should however be added, since according to the former arguments, the empty spin-up and -down d_{yz} bands should not be splitted at all.

IV. CHAINS OF TMCP₂ MOLECULES INSIDE CARBON NANOTUBES

A. Motivation and notation

Isolated metallocene chains clearly lack mechanical stability. We therefore propose that encapsulating them inside carbon nanotubes should provide the wanted isolation and stabilization. Inclusion of organic molecules inside carbon nanotubes entails however a series of stringent requirements. Encapsulation of individual molecules can surely be achieved if the chemical process is exothermic. But assumed this condition is fulfilled, the energy barriers for movement of the molecules along the axis of the nanotube should be tuned to be not too high to completely prevent this motion, nor too low to allow the molecules to displace freely. Notice that in this last case molecules should leave the tube under slight mechan-

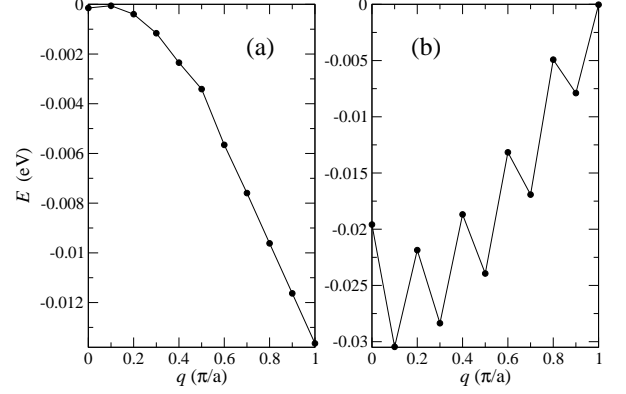


FIG. 3: Energy as a function of the spiral pitch vector for (a) an isolated chain of cobaltocenes and (b) a chain of cobaltocenes inside a (7,7) SWNT grown along the C_5 symmetry axis. $q = 0$ corresponds to the ferromagnetic configuration and $q = 1$ (in units of π/a) to the antiferromagnetic configuration.

ical shake-ups. Chain formation from the individual encapsulated molecules is helped by the own binding energy of the chain. This additional source of stabilization energy should link molecules together, and counteract the possible negative effect of the detuning of the energy barriers. Endothermic encapsulation of fullerenes has also been achieved²⁰. We therefore believe that individual metallocene molecules may be encapsulated by endothermic processes.

Encapsulation produces mechanical and electrical isolation of the metallocene chain. It also dopes the nanotube and produces local modifications of its band structure²⁰. These local modifications can be seen as electrostatic wells that trap electrons. We expect these traps to be deepest for endothermic encapsulation since in such a case the geometry would enhance the interaction between molecules and nanotube walls. Notice also that the length of the traps along the nanotube should be small for metallic nanotubes since in this case the screening length is pretty short. On the contrary, the length of the traps should be much larger for semiconducting nanotubes.

We wish to stress the importance of commensurating the lattice constant of the isolated chain (7.50 Å) with that of the nanotube, so that molecules accommodate well inside the tube and the chain is neither compressed nor strained. If the metallocene molecules are too close, electron clouds of two neighboring molecules will overlap too much and the full device is rendered endothermic. If they are too separated, then their wave functions won't overlap appreciably and the molecules can be considered as isolated. Since the unit cell of a armchair nanotube has a lattice constant of 2.50 Å, a metallocene may be well accommodated every three nanotube unit cells. The lattice constant of zigzag naotubes is 4.32 Å, so placing a molecule every two nanotube unit cells renders a stretched chain. Chiral tubes like the (12,4) or (15,5) have a lattice constant of 15.59 Å, and therefore one can safely place two metallocenes inside each of them to form a some-waht stretched chain. To avoid confusion, we use the following notation to denote the basic unit cell of the simulations:

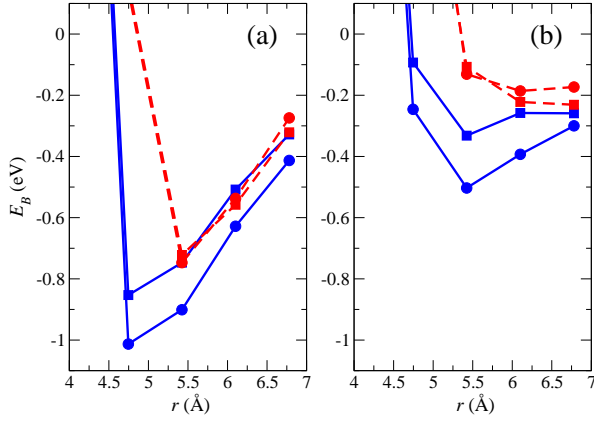


FIG. 4: Cohesive energy for the cases $N = 3$ (circles) and $N = 4$ (squares) in the parallel (continuous line) and perpendicular (broken line) configurations, calculated without (a) and with (b) BSSE correction.

$\# \text{TMCP}_2 @ N(n, n')$, where $\#$ is the number of metallocenes (TMCP_2) that are included in N unit cells of a (n, n') SWNT. We have also placed the molecules in two possible orientations, which we call parallel or perpendicular depending on whether the C_5 axis of the nanotube is aligned parallel or perpendicular to the nanotube axis.

B. Metallic nanotubes

We have found that the BSSE artificially enhances the stability of the encapsulated chains, so that BSSE corrections are essential to get right answers. This is explicitly shown in Fig. (4) for CoCp_2 chains, encapsulated in armchair tubes of different diameter. Notice that the most stable configuration corresponds to a (8,8), or (7,7) nanotubes (radii of 5.4 or 4.7 Å, respectively) depending on whether BSSE is corrected or not. Hence, we shall only discuss our results with BSSE correction, Fig. (4 (b)). We note that encapsulation is exothermic for armchair (n, n) tubes, with n equal or larger than 7 (radii equal or larger than 4.7 Å). The figure predicts that the highest rate of encapsulation should be achieved for (8,8) tubes, with smaller rates for (7,7), (9,9), (10,10) and so on. But the TEM images of Li *et al.*³⁷ only show encapsulation for radii similar to that of the (7,7) or slightly larger, and therefore predict a very selective encapsulation. We believe this is due to the small energy barriers that a metallocene would find when it moves along the axis of thicker tubes. Since experiments are performed at room temperature and samples are transported between different places, small barriers wouldn't prevent the metallocene to escape when mechanical and thermal perturbations increase its mobility.

Before switching to the analysis of the electronic structure we shall further analyze the results presented in Fig. (4 (b)). The figure demonstrates that molecules fit inside (7,7) tubes only if their axes are aligned. Misaligned molecules can be placed inside thicker tubes, but with a pretty large energy cost. We shall therefore only analyze aligned metallocene

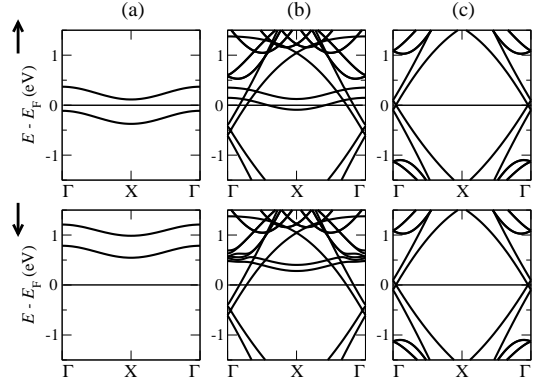


FIG. 5: Band structure of (a) an isolated cobaltocene chain (lattice constant = 7.5 Å), (b) a cobaltocene inside 3 unit cells of a (7,7) nanotube (the same separation between molecules as before) and (c) a (7,7) nanotube, for spin-up and spin-down electrons.

molecules in what follows. According to the same figure metallocenes can also lower significantly their energy by sticking close enough, which means that the most stable configuration corresponds to a molecular chain inside the nanotube. This is also confirmed experimentally by the TEM images of Li *et al.*³⁷, where the cobaltocenes show a clear tendency to appear together.

We turn now to discuss the electronic properties of the preferred $\text{CoCp}_2 @ 3(7,7)$ devices. The first remarkable property of these systems is a charge transfer of $0.6 e^-$ from the cobaltocene to the nanotube, which is due to the high electron affinity of the latter²⁴. Such a charge transfer, which is responsible for the reduction of the magnetic moment of the molecule from 1 to $0.4 \mu_B$, can also be inferred from the shift in the position of the spin-up d_{xz} band when the chain is inserted in the tube. This shift can be appreciated by comparing the band structures of isolated and encapsulated chains, that we depict in Figs. (5 (a), (b)). This transfer makes the valence bands of the nanotube move down, as can be seen in Figs. (5 (b), (c)). On the other hand the crystal field splitting of the Co d bands decreases from about 0.5 to 0.2 eV. This effect is mainly due to the change in the atomic positions of the encapsulated cobaltocene. Indeed, by plotting the bands of an isolated chain calculated using the coordinates of the cobaltocene in the $\text{CoCp}_2 @ 3(7,7)$ structure we find that the change in the crystalline field is very similar. The screening and charge transfer also produces a large reduction of the Stoner splitting from 1.3 to 0.5 eV. Taking the mean field estimate for this splitting, $\Delta E \approx nU = 0.4U$, gives a Hubbard U of 1.3 eV again. We therefore infer that screening effects produced by the nanotube do not reduce the Coulomb interaction in these chains.

The filling of the metallocene chains modifies the mean-field ground state, that was insulating and antiferromagnet in vacuum, to an helical state with a small pitch vector very close to the ferromagnetic solution, as can be appreciated in Fig. (3 (b)). The small oscillations in the energy are due to the application of the spiral rotation to the nanotube states.

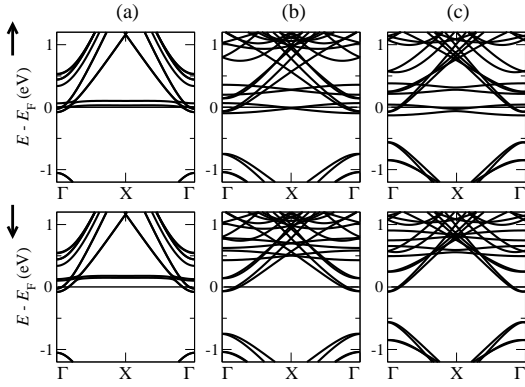


FIG. 6: Band structure of (a) $\text{CoCp}_2@2(11,0)$ (b) $2\text{CoCp}_2@(12,4)$ and (c) $2\text{CoCp}_2@(15,5)$ for spin up and spin down electrons.

C. Semiconducting nanotubes

We extend now the same discussion to the case of semiconducting nanotubes. The evolution of the binding energy and charge transfer to the nanotube wall as a function of the nanotube radius is very similar to the armchair case. Zigzag nanotubes start being exothermic for a radius of ~ 4.7 , which corresponds to the (12,0) tube. The chiral nanotubes (12,4) and (15,5), with radii of 5.7 and 7.2 Å respectively, have also been found to be exothermic. Furthermore, we have found that the charge transfer decreases as the radius of the nanotube increases, as in armchair tubes.

We show in Fig. (6) the band structures of $\text{CoCp}_2@2(11,0)$, $2\text{CoCp}_2@(12,4)$ and $2\text{CoCp}_2@(15,5)$ as representative of stretched and reasonably commensurated chains. The most noticeable feature in the first case, which corresponds to an endothermic encapsulation, is the severe reduction of the crystalline field between the d_{yz} and d_{xz} bands as a consequence of the change in the atomic positions produced by the strong interaction with the nanotube wall. Note also that these bands are almost non-dispersive due to the large separation between metallocenes along the nanotube axis, which are placed about 8.64 Å apart. The chiral cases are very similar, despite the large difference between their radii, although, as expected, the charge transfer is larger in the (12,4). In both cases the cobaltocene bands are clearly dispersive and show a crystalline field splitting which in the (15,5) is slightly larger due to the smaller interaction with the nanotube wall. Note that bands associated with the cobaltocene are folded due to the presence of two molecules in the unit cell.

The Hubbard U can not be cleanly estimated in the endothermic (11,0) encapsulation due to the strong modification of the cobaltocene bands and the hybridization with the nanotube states. However, in the chiral nanotubes by taking into account the exchange splittings, which are 0.72 and 0.87 eV in the (12,4) and (15,5), respectively, and the occupations of each spin up d_{xz} level, which are 0.57 and 0.67 electrons, respectively, U turns out to be again 1.3 eV, in agreement with the armchair nanotube. This demonstrates the robustness of the calculation.

V. MAPPING TO STRONGLY CORRELATED MODELS

A. Physics at the chain

The discussion following Figs. (2 (b)) and (5 (a), (b)) highlighted the similarities of the band structure, ground state and magnetism of isolated or encapsulated metallocene chains to strongly correlated Hubbard chains at diverse doping levels. We wish to take a closer look to this delicate issue now.

Indeed, an isolated metallocene chain may be viewed as a series of magnetic impurities stacked on top of each other, whose wave-functions have little overlap. The result of the process of encapsulation may therefore be a sort of Kondo chain, where the metallocene chain acts as an impurity lattice that hybridizes with the electronic (Luttinger) liquid residing in the host nanotube.

The parameters that tune the model are therefore the hybridizations among metallocene molecules V_{MM} , or between metallocenes and the nanotube V_{MN} . We note that V_{MM} is rather small for many of the isolated or encapsulated metallocene chains since these molecules are fairly stable and therefore do not like to share electrons. Exceptions are CoCp_2 and NiCp_2 , whose bandwidth are sizeable. We shall therefore confine the discussion below again to cobaltocene chains. In order to estimate the size of the nanotube-molecule hybridization integral V_{MN} , we first look into the band structure of the composite device in Fig. (5 (b)). The figure shows that the most important effect of encapsulation is a transfer of charge that shifts the metallocene bands upwards and the nanotube bands downwards, and, associated with it and with a change of atomic positions, a reduction of crystal field and exchange splittings. Nanotube and metallocene bands close to the Fermi level cross each other with no apparent hybridization. This fact indicates that V_{MN} is essentially zero. Additional confirmation comes from the fact that nanotube bands in the encapsulated device are not spin-split and therefore the nanotube does not magnetize.

We cross-check this estimate of the hybridization by taking a look at the projected density of states (PDOS) of the different molecule and nanotube atoms, which is plotted in Figs. (7), (8) and (9) for the cases of an isolated CoCp_2 and a (7,7) nanotube, a $\text{CoCp}_2@3(7,7)$ chain and a $\text{CoCp}_2@4(7,7)$ chain, respectively. All of these devices have been simulated for the same lattice constant, which is that of the nanotube. Comparison of Figs. (7) and (8)/(9) confirms our view that the main effect of encapsulation is a transfer of charge and a structural modification that brings about a reduction of crystal field and exchange splittings. Furthermore, the last panel in Figs. (8) and (9) shows no noticeable splitting of the spin-resolved DOS projected on the carbon atoms of the nanotube.

We further notice that the shape of the DOS of cobalt atoms does not change too much. The only noticeable changes appear in the energy range $[-8, -6]$ eV below the Fermi energy in the DOS projected on the hydrogen and carbon atoms. What remains to be seen is whether these modifications are due to structural deformation of the molecules and nanotube walls after encapsulation, or to hybridization between them. We note that the sharp resonances associated to hydrogen atoms

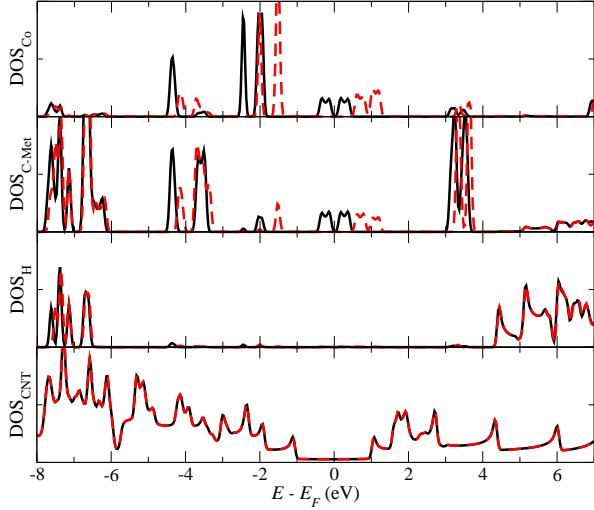


FIG. 7: From top to bottom, projected densities of states on the cobaltocene Co, C and H atoms for a Cobaltocene chain at its equilibrium distance, and a clean (7,7) SWNT. Solid and dashed lines indicate spin up and down components, respectively.

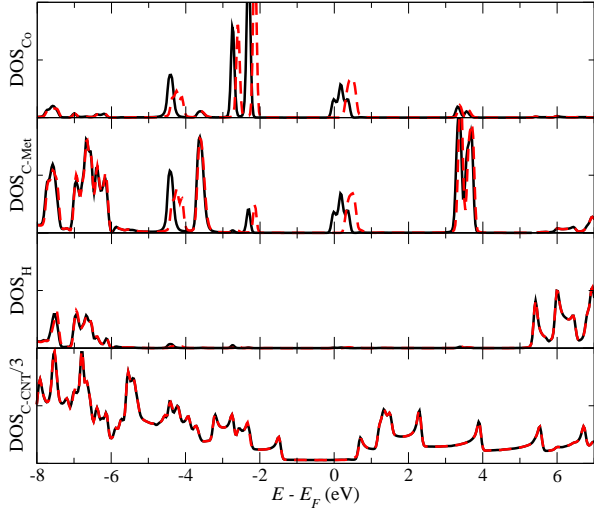


FIG. 8: From top to bottom, projected densities of states on the cobaltocene Co, C and H atoms and the nanotube walls in a CoCp₂@N(3,7) device. Solid and dashed lines indicate spin up and down components, respectively.

of the cobaltocene chain are clearly broadened after encapsulation. We therefore believe that Hydrogen atoms, and partly carbon atoms, do hybridize. This hybridization does have no implications in the electronic properties of the devices, since they appear well away the Fermi level. They provide a glue between molecules and tube, that hinders the axial motion of the molecule.

B. Physics at the walls

We now look at the change in the electrostatic potential at the nanotube walls created by the combined effect of charge transfer, structural modification, and hybridization with hydrogen atoms. We expect that the potential will show well-defined wells around the positions where the metallocene molecules are placed, that will be better or worse screened depending on the metallic or semiconducting character of the walls. These wells, that should trap electrons^{20,21}, will form a periodic chain with the same lattice constant as the underlying metallocene chain. A good estimate of the shape, length and depth of these wells, can be provided by calculating the electrostatic potentials at the walls of the nanotube of a CoCp₂@N(*n*, *n'*) device with and without metallocene molecules, and subtracting one from the other, $\Delta V(z) = V_{H,with}(z) - V_{H,without}(z)$. We note that this potential should have axial symmetry and hence only depend on the *z*-coordinate.

We have checked that ΔV is rather small for metallic devices since, as expected, the valence electrons at the walls screen the charge perturbation efficiently. We have subsequently looked into the semiconducting CoCp₂@N(11,0) device (radius of 4.4 Å), whose band structure is plotted in Fig. (6 (a)). In this case the encapsulation is endothermic and therefore the modification of the potential is expected to be further enhanced as a consequence of the strong interaction between the metallocene and the nanotube wall. Indeed we have found that the potential barrier is rather large as can be seen in Fig. (10), where we plot ΔV as a function of the axial coordinate for a device where *N* = 2 and for another where *N* = 4. We note that we have placed one molecule at the origin of the *z*-coordinate. We immediately note the periodicity in ΔV for both *N* = 2 (8.6 Å) and *N* = 4 (17.2 Å). The potential has two symmetric minima, placed at the positions of the close-by *C*₅ rings and a maximum in between them, that corresponds to the position of the cobalt atom, which is farther apart. The absolute maximum in $\Delta V(z)$ appears at the middle point between two molecules. The height of the well depends on both the lattice constant of the chain and the screening length. The figure shows that $\Delta V(z)$ has enough room to reach zero when *N* = 4, allowing us to estimate a value of about 6-7 Å for the screening length. For *N* = 2, on the contrary, the distance between wells (8.6 Å) is not long enough to allow the complete healing of the potential. Accordingly, the depth of the well decreases from 0.2 to 0.1 eV.

VI. TRANSPORT PROPERTIES OF ISOLATED METALLOCENES INSIDE CARBON NANOTUBES

The case where cobaltocenes form a chain inside the nanotube⁴⁴ can lead to magnetoresistive ratios of 20% due to the suppression of the spin channel that goes through the molecular chain. A different situation however is that produced when a cobaltocene sits in between two infinite nanotube electrodes, as shown in Fig. (11).

The conductance of such a system is plotted in Fig. (12) for

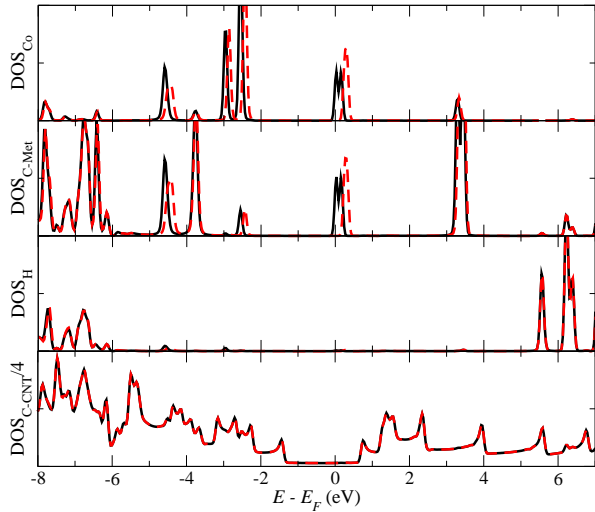


FIG. 9: From top to bottom, projected densities of states on the cobaltocene Co, C and H atoms and the nanotube walls in a $\text{CoCp}_2@4(7,7)$ device. Solid and dashed lines indicate spin up and down components, respectively.

three different metallocenes, namely ferrocene, cobaltocene and nickelocene in the parallel configuration. These are representative cases since the other metallocenes, with the possible exception of the ruthenocene and the osmocene, have smaller dimensions and are expected to produce less interaction with the nanotube wall. The transmission of the clean nanotube is also plotted for comparison. As can be seen the net effect produced on the transmission coefficients by isolated metallocenes is not very large and the transmission at the Fermi level is not affected. Notice that in the case of the magnetic molecules the transmission is exactly the same for spin-up and spin-down electron due to the fact that the carbon nanotube does not acquire any spin polarization from the charge that is transferred from the metallocene. The only differences with a clean nanotube appear above and below the Fermi level and have the effect of rounding the transmission coefficients where the number of channels increases. This effect is mainly due to the structural deformation induced by the metallocene rather than to any electronic influence, although it could also be due to the charge transfer. The change seems to be very small for the ferrocene impurity whereas the cobaltocene produces the largest modifications.

We therefore predict that there should be no change in the transport measurements of isolated metallocenes inside nanotubes with radii larger 4.5 \AA , unless the applied voltage is large enough ($> 2 \text{ V}$) to reach the regions with large number of channels. In such a case the presence of scattering would decrease the measured current and conductance and this effect would be clearly seen in the second derivative of the current with respect to the voltage. It is also worth mentioning that such an effect would be more pronounced in nanotubes with small diameter but the encapsulation of metallocenes would be difficult to realize due to the endothermic character, which would probably produce defects that would have a larger influence on the transport properties.

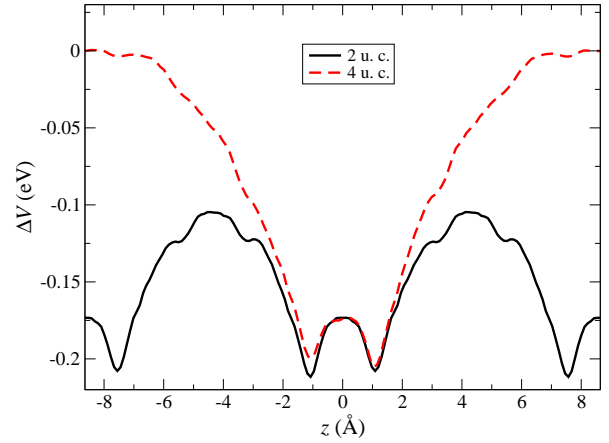


FIG. 10: ΔV as a function of the z -coordinate for $\text{CoCp}_2@2(11,0)$ (continuous line) and $\text{CoCp}_2@4(11,0)$ (dashed line) devices.

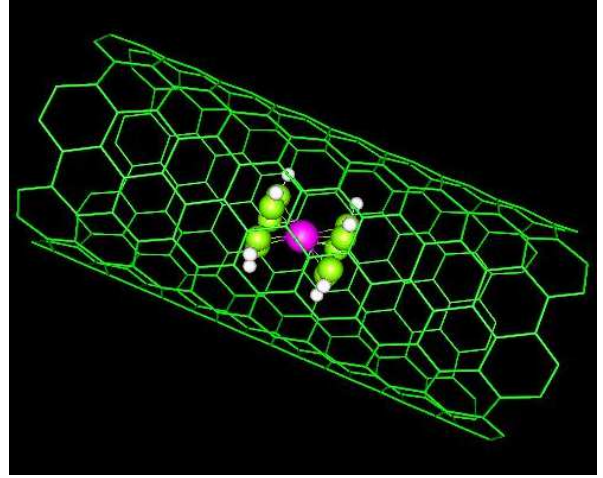


FIG. 11: Unit cell used to calculate the transport properties of a clean nanotube with a metallocene impurity. The atoms of the metallocene have been highlighted for clarity.

VII. CONCLUSIONS

We have shown that density functional theory in combination with pseudopotentials and linear combinations of atomic orbitals provides a very accurate description of the electronic and structural properties of metallocenes, whose results are in excellent agreement with experiments. The electronic configuration of metallocenes, which is mainly determined by the interplay between the crystalline field splitting and Hund's rules on the d bands, shows a kind of mirror symmetry with respect to the column of iron due to the number of unpaired electrons. The filling of the d bands and the shape and symmetry of the orbitals involved can also explain the distribution of the structural parameters as a function of the repulsion between the orbitals of the cyclopentadienyl rings and those of the transition metal atom. As a consequence the metallocenes become bigger as the number of electrons of the metallic atom increases.

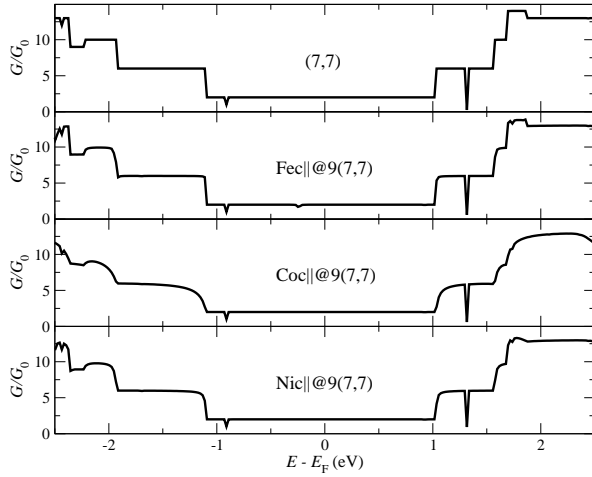


FIG. 12: Transmission coefficients of isolated ferrocenes, cobaltocenes and nickelocenes in the parallel configuration between semi-infinite (7,7) SWNT leads. For comparison it is also shown the transmission coefficients of a clean (7,7) SWNT.

The electronic configuration of metallocene chains does not differ too much from that of the isolated metallocenes, the main difference being the finite dispersion of the states around the Fermi level, which make them conducting. Such states, which in the cobaltocene are half-filled are responsible for the magnetic configuration of the chains, which we demonstrated to be antiferromagnetic by calculating the energy of a series of helical configurations with the help of the generalized Bloch's theorem. The spin polarization of those states makes these systems perfect candidates for spintronics applications. However, it is necessary to look for possible methods to stabilize them without destroying such interesting properties.

The most obvious way of producing stable metallocene chains is by placing them inside a carbon nanotube, which would act as an external coating that would protect them mechanically and electrically. Such a system was found to be exothermic for radii larger than 4.5 Å, in agreement with recent experiments. The encapsulated metallocenes produce a transfer to the nanotube wall and the carbon nanotube be-

comes n -doped. This effect is clearly seen when the band structure or the density of states of the composite system is analyzed. Such charge transfer changes also the most stable magnetic configuration which moves close to the ferromagnetic point with a small spiral pitch vector, although the difference in energy is small enough to point all spins up with the application of a magnetic field. By closely analyzing the projected density of states it is also possible to study the interaction of the molecular magnetic moment with the conduction electrons of the carbon nanotube.

Our mean-field calculations show that CoCp₂ chains behave as strongly correlated electron liquids, that can be perfectly well described by a half-filled Hubbard model. We further note that the hopping t and Coulomb U parameters can be univocally extracted from our simulations. We also show that encapsulation only produces a charge transfer that carries the Hubbard liquid away from half-filling.

Looking into the effects on the nanotube walls, we have shown that encapsulation inside semiconducting nanotube produces deep wells in the electrostatic potential that should act as quantum dots that trap electrons.

Finally, we also studied the transport characteristics of metallocenes between semi-infinite clean nanotubes. We found that the transmission coefficients do not change too much with respect to the transmission coefficients of a clean nanotube, the only difference being the rounding of the steps where the number of channels increases. This would give rise to changes in the second derivative of the current with respect to the voltage for large bias voltages.

Acknowledgments

We would like to thank John H. Jefferson for useful and stimulating discussions. We acknowledge financial support from the UE network MRTN-CT-2003-504574 RTNNANO, the Spanish project MEC BFM2003-03156 and the UK EPSRC. VMGS thanks the European Union for a Marie Curie grant.

- ¹ S. Iijima, *Nature (London)* **354**, 56 (1991).
- ² P. R. Bandaru, C. Daraio and A. M. Rao, *Nature Materials* **4**, 663 (2005).
- ³ M. S. Dresselhaus, G. Dresselhaus, and R. Saito, *Physical Properties of Carbon Nanotubes* (Imperial College, London, 1998).
- ⁴ S. J. Tans, A. R. M. Verschueren, and C. Dekker, *Nature (London)* **393**, 49 (1998).
- ⁵ Z. Yao, H. W. Ch. Postma, L. Balents, and C. Dekker, *Nature (London)* **402**, 273 (1999).
- ⁶ H. W. Ch. Postma, T. Teepen, Z. Yao, M. Grifoni, and C. Dekker, *Science* **293**, 76 (2001).
- ⁷ S. Kazaoui, N. Minami, R. Jacquemin, H. Kataura, and Y. Achiba, *Phys. Rev. B* **60**, 13339 (1999).
- ⁸ C. W. Zhou, J. Kong, E. Yenilmez, and H. J. Dai, *Science* **290**,

- ⁹ P. Collins, K. Bradley, M. Ishigami, and A. Zettl, *Science* **287**, 622 (2000).
- ¹⁰ E. Jouguelet, C. Mathis, and P. Petit, *Chem. Phys. Lett.* **318**, 561 (2000).
- ¹¹ J. Kong and H. J. Dai, *J. Phys. Chem. B* **105**, 2890 (2001).
- ¹² R. Martel, V. Derycke, C. Lavoie, J. Appenzeller, K. K. Chan, J. Tersoff, and P. Avouris, *Phys. Rev. Lett.* **87**, 256805 (2001).
- ¹³ S. Kazaoui, N. Minami, N. Matsuda, H. Kataura, and Y. Achiba, *Appl. Phys. Lett.* **78**, 3433 (2001).
- ¹⁴ M. Shim, A. Javey, N. W. S. Kam, and H. J. Dai, *J. Am. Chem. Soc.* **123**, 11512 (2001).
- ¹⁵ V. Derycke, R. Martel, J. Appenzeller, and P. Avouris, *Appl. Phys. Lett.* **80**, 2773 (2002).
- ¹⁶ A. Javey, H. Kim, M. Brink, Q. Wang, A. Ural, J. Guo, P. McIn-

- tre, P. McEuen, M. Lundstrom, and H. J. Dai, *Nat. Mater.* **1**, 241 (2002).
- ¹⁷ S. C. Tsang, Y. K. Chen, P. J. F. Harris, and M. L. H. Green, *Nature* **372**, 159 (1994).
 - ¹⁸ C. Guerret-Piécourt, Y. Le Bouar, A. Loiseau, and H. Pascard, *Nature* **372**, 761 (1994).
 - ¹⁹ D. J. Hornbaker, S.-J. Kahng, S. Misra, B. W. Smith, A. T. Johnson, E. J. Mele, D. E. Luzzi, and A. Yazdani, *Science* **295**, 828 (2002).
 - ²⁰ J. Lee, H. Kim, S.-J. Kahng, G. Kim, Y.-W. Son, J. Ihm, H. Kato, Z. W. Wang, T. Okazaki, H. Shinohara, and Young Kuk, *Nature* **415**, 1005 (2002).
 - ²¹ Y. Cho, S. Han, G. Kim, H. Lee, and J. Ihm, *Phys. Rev. Lett.* **90**, 106402 (2003).
 - ²² D. Gunlycke, J. H. Jefferson, T. Rejec, A. Ramšak, D. G. Pettifor and G. A. D. Briggs, *J. Phys.: Condens. Matter* **18**, S851 (2006).
 - ²³ T. Takenobu, T. Takano, M. Shiraishi, Y. Murakami, M. Ata, H. Kataura, Y. Achiba, and Y. Iwasa, *Nat. Mater.* **2**, 683 (2003).
 - ²⁴ J. Lu, S. Nagase, D. Yu, H. Ye, R. Han, Z. Gao, S. Zhang, and L. Peng, *Phys. Rev. Lett.* **93**, 116804 (2004).
 - ²⁵ V. Pinoch, P. Launois, M. Pinault, M. Mayne-L'Hermite, and C. Reynaud, *Appl. Phys. Lett.* **85**, 473 (2004).
 - ²⁶ S. Karmakar, S. M. Sharma, P. V. Teredesai, and A. K. Sood, *Phys. Rev. B* **69**, 165414 (2004).
 - ²⁷ C. Prados, P. Crespo, J. M. González, A. Hernando, J. F. Marco, R. Gancedo, N. Grobert, M. Terrones, R. M. Walton, and H. W. Kroto, *Phys. Rev. B* **65**, 113405 (2002).
 - ²⁸ S. Karmakar, S. M. Sharma, M. D. Mukanadam, S. M. Yusuf, and A. K. Sood, *J. Appl. Phys.* **97**, 054306 (2005).
 - ²⁹ R. Che, L.-M. Peng, X. Duan, Q. Chen, and X. Liang, *Adv. Mater. (Weinheim, Ger.)* **16**, 401 (2004).
 - ³⁰ B. C. Satishkumar, A. Govindaraj, P. V. Vanitha, A. K. Raychaudhuri, and C. N. R. Nao, *Chem. Phys. Lett.* **362**, 301 (2002).
 - ³¹ T. Mühl, D. Elefant, A. Graff, R. Kozhuharova, A. Leonhardt, I. Mönch, M. Ritschel, P. Simon, S. Groudeva-Zotova, and C. M. Schneider, *J. Appl. Phys.* **93**, 7894 (2003).
 - ³² J. W. Jang, K. W. Lee, C. E. Lee, T. J. Lee, C. J. Lee, and S. C. Lyu, *Phys. Stat. Sol.* **241**, 1605 (2004).
 - ³³ C.-K. Yang, J. Zhao, and J. P. Lu, *Phys. Rev. Lett.* **90**, 257203 (2003).
 - ³⁴ Y. Yagi, T. M. Briere, M. H. F. Sluiter, V. Kumar, A. A. Farajian, and Y. Kawazoe, *Phys. Rev. B* **69**, 075414 (2004).
 - ³⁵ M. Weissmann, G. García, M. Kiwi, and R. Ramírez, *Phys. Rev. B* **70**, 201401(R) (2004).
 - ³⁶ M. Weissmann, G. García, M. Kiwi, R. Ramírez, and C.-C. Fu, *Phys. Rev. B* **73**, 125435 (2006).
 - ³⁷ L.-J. Li, A. N. Khlobystov, J. G. Wiltshire, G. A. D. Briggs, R. J. Nicholas, *Nature Materials* **4**, 481 (2005).
 - ³⁸ A. Togni and R. L. Halterman, *Metalloenes : synthesis, reactivity, applications* (John Wiley and Sons, New York 1998).
 - ³⁹ N. J. Long, *Metalloenes: An Introduction to Sandwich Complexes* (Blackwell Science, London 1998).
 - ⁴⁰ C. Engtrakul and L. R. Sita, *Nano Lett.* **1**, 541 (2001).
 - ⁴¹ S. A. Getty, C. Engtrakul, L. Wang, R. Liu, S.-H. Ke, H. U. Baranger, W. Yang, M. S. Fuhrer, and L. R. Sita, *Phys. Rev. B* **71**, 241401(R) (2005).
 - ⁴² R. Liu, S.-H. Ke, H. U. Baranger, and W. Yang, *Nano Lett.* **5** 1959 (2005).
 - ⁴³ R. Liu, S.-H. Ke, W. Yang, and H. U. Baranger, *J. Chem. Phys.* **124** 024718 (2006).
 - ⁴⁴ V. M. García-Suárez, J. Ferrer, and C. J. Lambert, *Phys. Rev. Lett.* **96**, 106804 (2006).
 - ⁴⁵ W. Kohn and L. J. Sham, *Phys. Rev.* **140**, A1133 (1965).
 - ⁴⁶ J. M. Soler, E. Artacho, J. D. Gale, A. García, J. Junquera, P. Ordejón, and D. Sánchez-Portal, *J. Phys.: Condens. Matter* **14**, 2745 (2002).
 - ⁴⁷ N. Troullier and J. L. Martins, *Phys. Rev. B* **43**, 1993 (1991).
 - ⁴⁸ O. F. Sankey and D. J. Niklewski, *Phys. Rev. B* **40**, 3979 (1989).
 - ⁴⁹ S. G. Louie, S. Froyen, and M. L. Cohen, *Phys. Rev. B* **26**, 1738 (1982).
 - ⁵⁰ V. M. García-Suárez, C. M. Newman, C. J. Lambert, J. M. Pruneda, and J. Ferrer, *Eur. Phys. J. B* **40**, 371 (2004).
 - ⁵¹ V. M. García-Suárez, C. M. Newman, C. J. Lambert, J. M. Pruneda, and J. Ferrer, *J. Phys.: Condens. Matter* **16**, 5453 (2004).
 - ⁵² S. F. Boys and F. Bernardi, *Mol. Phys.* **19**, 553 (1970).
 - ⁵³ E. D. Glendening, *J. Am. Chem. Soc.* **118**, 2473 (1996).
 - ⁵⁴ W. A. Herrebout, J. Lundell, and B. J. Van der Veken, *J. Phys. Chem. A* **102**, 10173 (1998).
 - ⁵⁵ J. P. Perdew, K. Burke, and M. Ernzerhof, *Phys. Rev. Lett.* **77**, 3865 (1996).
 - ⁵⁶ A. R. Rocha, V. M. García-Suárez, S. W. Bailey, C. J. Lambert, J. Ferrer and S. Sanvito, *Nat. Mat.* **4**, 335 (2005).
 - ⁵⁷ A. R. Rocha, V. M. García-Suárez, S. Bailey, C. Lambert, J. Ferrer and S. Sanvito, *Phys. Rev. B* **73**, 085414 (2006).
 - ⁵⁸ L. V. Keldysh, *Sov. Phys. JETP* **20**, 1018 (1965).
 - ⁵⁹ H. Eicher, *Phys. Rev. A* **40**, 1637 (1989).
 - ⁶⁰ D. S. Fisher and P. A. Lee, *Phys. Rev. B* **23** R6851 (1981).